IEEE Access
Multidisciplinary | Rapid Review | Open Access Journal

Received September 20, 2019, accepted October 21, 2019, date of publication November 7, 2019,
date of current version December 2, 2019.

Digital Object Identifier 10.1109/ACCESS.2019.2950732

Joint DOA and Polarization Estimation via Canonical Polyadic Decomposition With Constant Modulus Constraints

JIN-WEI YANG[1], XIAO-FENG GONG[1], (Member, IEEE), CHEN-YU XU[1], QIU-HUA LIN[1], (Member, IEEE), YOU-GEN XU[2], (Member, IEEE), AND ZHI-WEN LIU[2], (Member, IEEE)

[1]School of Information and Communication Engineering, Dalian University of Technology, Dalian 116023, China
[2]School of Information and Electronics, Beijing Institute of Technology, Beijing 100081, China

Corresponding author: Xiao-Feng Gong (xfgong@dlut.edu.cn)

This work was supported in part by the National Natural Science Foundation of China under Grant 61671106, Grant 61331019, Grant 61490691, and Grant 61871067.

ABSTRACT We consider the joint estimation of direction-of-arrival (DOA) and polarization of constant modulus (CM) signals based on an electromagnetic vector-sensor (EMVS) array. Two algebraic algorithms for canonical polyadic decomposition (CPD) with CM constraint are proposed in two scenarios, in which the source signals are fully and partially CM, respectively. The proposed algorithms use the analytic CM algorithm in the first step to calculate the source matrix, and then exploit the CPD structure of the data tensor to compute the remaining factor matrices, from which the DOA and polarization parameters can finally be obtained. Due to the algebraic nature, the proposed algorithms are faster and more stable than the optimization based algorithms, and can be used to effectively initialize the latter. We have shown that the proposed algorithms have more relaxed uniqueness conditions than unconstrained CPD, and thus can be applied in highly underdetermined cases where the number of source signals greatly exceeds that of the EMVSs. Simulation results are provided to illustrate the performance of the proposed algorithms.

INDEX TERMS Direction-of-arrival, polarization, tensor, canonical polyadic decomposition, constant modulus.

I. INTRODUCTION

An electromagnetic vector-sensor (EMVS) comprises $2-6$ electromagnetic (EM) sensors (e.g., orthogonally oriented short dipoles and/or small loops arranged in a co-located or distributed manner, see FIGURE 1) that provide complete or partial measurements of the EM fields induced by the incident sources [1]–[5]. An EMVS array consists of multiple EMVSs, arranged into a certain spatial configuration, e.g. linear, circular, L-shaped. Compared with the conventional scalar sensor array, which mainly captures and exploits the information of signals in the time-space domain, an EMVS array can additionally perceive the diversity of impinging signals in the polarization domain. Therefore, an EMVS array is polarization sensitive. As such, during the past several decades, there have been enormous efforts devoted to the development of direction-of-arrival (DOA) and polarization estimation techniques based on the EMVS array [6]–[20]. These works have revealed the advantages of EMVS array over scalar sensor array, with regard to parameter estimation accuracy, identifiability, etc.

As mentioned above, the EMVS array output signal admits a multi-dimensional (MD) structure in the time-space-polarization domain. For example, we can express the observed signal of an EMVS array as an $N \times K \times T$ tensor $\boldsymbol{\mathcal{X}}$, where N, K, T denote the dimensionality of the signal in space, polarization, and time domain, respectively. As such, a particular entry of $\boldsymbol{\mathcal{X}}$, $x_{n,k,t}$, denotes the array signal associated with the kth component of the nth EMVS, at time instant t. However, the early methods, such as multiple signal classification (MUSIC) [12]–[14] and estimation of signal parameters via rotational invariance techniques (ESPRIT) [15]–[20], do not fully exploit this MD structure. More precisely, the MUSIC based techniques employ a long-vector

The associate editor coordinating the review of this manuscript and approving it for publication was Wei Liu.

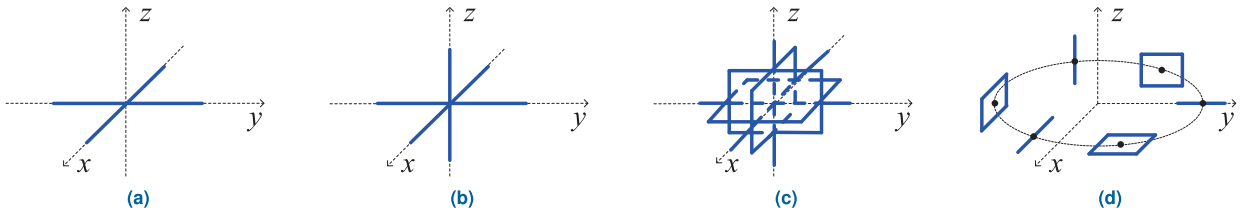

FIGURE 1. Illustration of four typical EMVSs. (a) Cross-dipole. (b) Triple. (c) The cocentered complete EMVS. (d) The distributed complete EMVS.

model, which combines the space and polarization modes of an EMVS array data, i.e. they do not distinguish the space and polarization domain. The ESPRIT based approaches, on the other hand, divide the EMVS array into two or more subarrays, and exploit the rotational invariance property between them. These approaches do not fully make use of the MD structure, in the sense that the number of signals that can be handled by ESPRIT is required to be less than the number of sensors in each subarray.

Tensor based methods for array processing were proposed in the past decades. In [9], [21]–[23], the conventional matrix based subspace methods are extented to the higher-order case. These methods use the multilinear singular value decomposition and low multilinear (ML) rank approximtion in the estimation of ML subspaces, and are shown to perform better than their matrix based counterpart. In [21]–[23], the canonical polyadic decomposition (CPD) of third order tensor, also known as parallel factor analysis or canonical decomposition, is used for DOA estimation based on a multi-invariance array. Third-order and fourth-order CPDs is widely adopted in a number of EMVS array processing techniques, which are shown to have better performance than the matrix based approaches.

The above methods are mainly based on unconstrained tensor decompositions. In practice, however, prior knowledge of either the source signal or the sensor array is often available. Imposing these priors in tensor decomposition as certain structure or constraint may result in better performance with regard to both accuracy and identifiability [24]–[27]. Commonly used structures/constraints include orthogonality [24], non-negativity [25], Vandermonde structure [26], Toeplitz structure [27], etc, and a variety of constrained tensor decomposition algorithms have been developed in the literature. Notably, a library of tensor decompositions and factor structures/constraints to choose from, as well as a flexible framework of structured data fusion (SDF) for structured/coupled matrix and tensor decomposition, is offered in Tensorlab 3.0 [28].

In this study, we consider DOA and polarization estimation of constant modulus (CM) signals based on an EMVS array, using CM constrained CPD.CM signals are widely used in practice. For example, the BPSK, QPSK and 8PSK signals are adopted in relay satellite communication systems. Even in the receive array scenario, where the receive signals are not strictly CM due to channel attenuation, it is still reasonable to consider approximate CM signals. Indeed, many existing works have considered the scenario where the receive array signals are CM signals or multi-modulus (MM) signals, and have proposed a lot of algorithms exploiting the CM or MM properties [29], [30]. However, existing work on CM signal processing did not consider the use of EMVS arrays where the received signals admit a CPD model. Moreover, existing work on CPD did not discuss how CM property can be used to relax the uniqueness conditions of a CPD. Based on the above reasons, we think it is of practical significance to study the CM property with EMVS array. By applying the analytic CM algorithm (ACMA) [30] and imposing the CPD structure, we present two algebraic CPD algorithms with full and partial CM constraints, which correspond to the following two scenarios, respectively: (a) all the sources are CM signals; (b) part of the sources are CM signals. We also present a joint DOA and polarization estimator which jointly exploits the factor matrices in both space and polarization modes. The proposed algorithms are algebraic. Therefore, they are computationally efficient and stable, and can be used to effectively initialize the optimization based algorithms (e.g., the SDF implementation of a CPD with CM constraints). The main advantage of the proposed algorithms, in comparison with the unconstrained CPD, which will be clarified later, is that the CM constraint can further relax the uniqueness conditions of a CPD. Put it into the context of EMVS array, the above advantage implies that by using CM property an EMVS array may identify the DOA and polarization parameters of more source signals. In addition, through simulations we have found that the proposed algorithms can generate correct results even in cases where the unconstrained CPD is not unique.

The rest of the paper is organized as follows. In Section II, we introduce the data model of an EMVS array receiving CM signals, and formulate the jont DOA-polarization estimation problem as a CPD with CM constraints. In Section III, we propose two CPD algorithms with full and partial CM constraints, respectively, and present a joint DOA-polarization estimator. In Section IV, simulation results are given to illustrate the performance of the proposed algorithms, in comparison with optimization based algorithms, implemented with SDF, and unconstrained CPD. Section V concludes the paper.

We note that part of the results of the paper, i.e., the full CM constraint based method, has been presented in [31] as a conference paper.

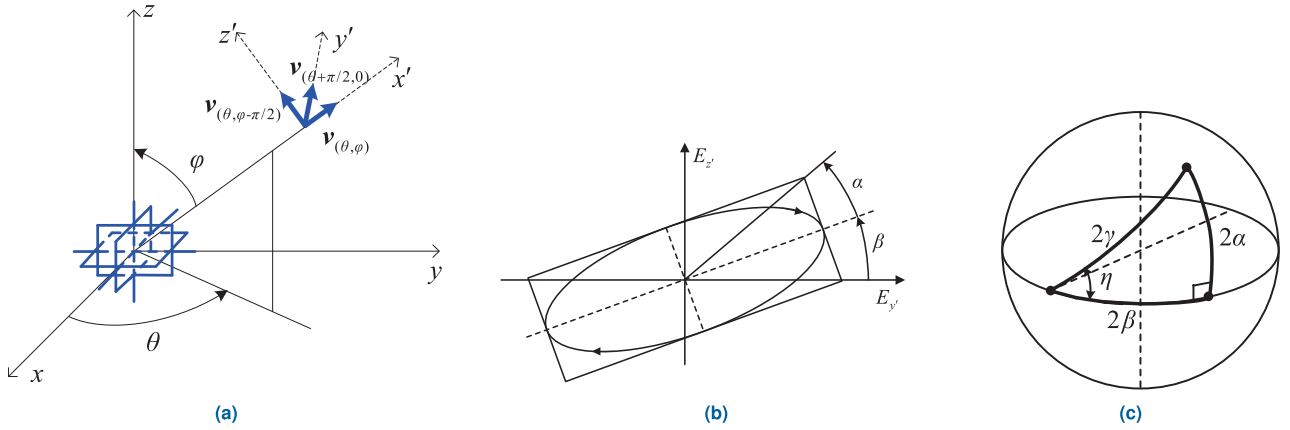

FIGURE 2. The angle and polarization definition. (a) The angle definition. (b) Polarization ellipse. (c) Poincare sphere.

Notation: Scalars, vectors, matrices and tensors are denoted by italic lowercase, lowercase boldface, uppercase boldface and uppercase calligraphic letters, respectively. The rth column vector and the (i,j)th entry of $\boldsymbol{X}$ are denoted by $\boldsymbol{x}_r$ and $x_{i,j}$, respectively. The identity matrix and all-zero vectors are denoted by $\boldsymbol{I}_M \in \mathbb{R}^{M\times M}$ and $\boldsymbol{0}_M \in \mathbb{R}^{M\times M}$, respectively. The null space of a matrix $\boldsymbol{X}$ is denoted as $\ker(\boldsymbol{X})$. The dimensionality of a vector space $\Im$ is denoted as $\dim(\Im)$. Transpose, conjugate, conjugated transpose, Moore-Penrose pseudo-inverse, Frobenius norm and matrix determinant are denoted as $(\cdot)^T$, $(\cdot)^*$, $(\cdot)^H$, $(\cdot)^\dagger$, $\|\cdot\|_F$, and $|\cdot|$, respectively.

The symbols '$\otimes$', '$\odot$' and '$\circledast$' denote Kronecker product, Khatri-Rao product, and outer product, respectively. The symbol '$\wedge$' denotes vector-cross-product, defined as $a\wedge b \triangleq [a_2b_3-a_3b_2, a_3b_1-a_1b_3, a_1b_2-a_2b_1]^T$, $a,b\in\mathbb{C}_3$. The symbol '$\angle$' denotes the phase angle of a complex number, and 'im$(\cdot)$' denotes the imaginary part of its entry. The letter 'i' denotes the imaginary unit.

A polyadic decomposition (PD) of $\boldsymbol{\mathcal{X}}$ expresses $\boldsymbol{\mathcal{X}}$ as the sum of rank-1 terms:

$$\boldsymbol{\mathcal{X}} = \sum_{r=1}^{R} \boldsymbol{a}_r \circledast \boldsymbol{b}_r \circledast \boldsymbol{c}_r = [\![\boldsymbol{A},\boldsymbol{B},\boldsymbol{C}]\!]_R, \tag{1}$$

where $\boldsymbol{A} \triangleq [\boldsymbol{a}_1,\cdots,\boldsymbol{a}_R]\in\mathbb{C}^{I\times R}$, $\boldsymbol{B}\triangleq[\boldsymbol{b}_1,\cdots,\boldsymbol{b}_R]\in\mathbb{C}^{J\times R}$, and $\boldsymbol{C}\triangleq[\boldsymbol{c}_1,\cdots,\boldsymbol{c}_R]\in\mathbb{C}^{K\times R}$. We call (1) a canonical PD (CPD) if R is minimal.

For a matrix $\boldsymbol{A}\in\mathbb{C}^{I_1\times I_2}$, $\mathrm{vec}(\boldsymbol{A})\in\mathbb{C}^{I_1I_2}$ denotes the vector representation of $\boldsymbol{A}$: $[\mathrm{vec}(\boldsymbol{A})]_{\tilde{i}} \triangleq a_{i_1,i_2}$, with $\tilde{i}=(i_1-1)I_1+i_2$, while unvec$(\cdot)$ performs the inverse. The matrix representation [1] of $\boldsymbol{\mathcal{X}}\in\mathbb{C}^{I\times J\times K}$ is denoted as $\boldsymbol{X}\in\mathbb{C}^{IJ\times K}$, and defined by $\boldsymbol{X}_{((i-1)J+j,k)}=\boldsymbol{\mathcal{X}}_{(i,j,k)}$.

We define $\mathrm{Ten}(\boldsymbol{X},[I,J,K]) = \boldsymbol{\mathcal{X}}$ as the operation to reshape an $IJ\times K$ matrix $\boldsymbol{X}$ into a third-order $\boldsymbol{\mathcal{X}}$ of size $I\times J\times K$, such that $x_{i,j,k}=\boldsymbol{X}_{((i-1)J+j,k)}$. We denote the estimate of a variable $\boldsymbol{a}$ as $\tilde{\boldsymbol{a}}$.

[1]Note that there are various types of matrix representation of a third-order tensor, and that the one defined here is indeed the mode-3 matrix representation. In this paper we only consider this type of matrix representation.

II. DATA MODEL AND PROBLEM FORMULATION

A. DATA MODEL

Let (θ,φ) be the azimuth-elevation 2D DOA of a narrowband planar EM signal, (γ,η) be the polarization state of the incident signal, where γ and η denote the polarization auxiliary angle and the polarization phase difference, respectively, $0\le\theta<2\pi$, $0\le\varphi<\pi$, $0\le\gamma<\pi/2$, $-\pi\le\eta<\pi$ (see FIGURE 2 for the definition of DOA and polarization parameters). The response of a cocentered EMVS can be written as [2]:

$$\boldsymbol{b}_{\theta,\varphi,\gamma,\eta} \triangleq \boldsymbol{L}\begin{bmatrix}\boldsymbol{e}_{\theta,\varphi,\gamma,\eta}\\ \boldsymbol{h}_{\theta,\varphi,\gamma,\eta}\end{bmatrix}, \tag{2}$$

where

$$\begin{bmatrix}\boldsymbol{e}_{\theta,\varphi,\gamma,\eta}\\ \boldsymbol{h}_{\theta,\varphi,\gamma,\eta}\end{bmatrix} = \begin{bmatrix}\boldsymbol{v}_{(\theta+\pi/2,0)}, -\boldsymbol{v}_{(\theta,\varphi-\pi/2)}\\ \boldsymbol{v}_{(\theta,\varphi-\pi/2)}, \boldsymbol{v}_{(\theta+\pi/2,0)}\end{bmatrix}\begin{bmatrix}\cos\gamma\\ \sin\gamma e^{\mathrm{i}\eta}\end{bmatrix}, \tag{3}$$

where $\boldsymbol{e}_{\theta,\varphi,\gamma,\eta}\in\mathbb{C}^3$ and $\boldsymbol{h}_{\theta,\varphi,\gamma,\eta}\in\mathbb{C}^3$ are vectors holding the electric field components and magnetic field components of the incident EM waves, respectively. The vector $\boldsymbol{v}_{(\theta,\varphi)}\triangleq[\cos\theta\sin\varphi,\sin\theta\sin\varphi,\cos\varphi]^T$ denotes the Poynting vector associated with (θ,φ) (see FIGURE 2a). By definition, $\boldsymbol{v}_{(\theta,\varphi)}$, $\boldsymbol{v}_{(\theta+\pi/2,0)}$, $\boldsymbol{v}_{(\theta,\varphi-\pi/2)}$ constitute a mutually orthogonal triad as shown in FIGURE 2a. We denote $\boldsymbol{b}_{\theta,\varphi,\gamma,\eta}$ as the angular-polarization steering vector.

The binary matrix $\boldsymbol{L}\in\mathbb{R}^{K\times 6}$ is a selection matrix. It chooses a subset of the complete EM field components according to the type of the employed EMVS. For example, if the complete EMVS is used, then $\boldsymbol{L}=\boldsymbol{I}_6$ and $\boldsymbol{b}_{\theta,\varphi,\gamma,\eta}=[\boldsymbol{e}^T_{\theta,\varphi,\gamma,\eta},\boldsymbol{h}^T_{\theta,\varphi,\gamma,\eta}]^T$. If the tripole antenna is used, then $\boldsymbol{L}=[\boldsymbol{I}_3,\boldsymbol{0}_3]$ and $\boldsymbol{b}_{\theta,\varphi,\gamma,\eta}=\boldsymbol{e}_{\theta,\varphi,\gamma,\eta}$.

Now we introduce the data model of an array of N EMVSs. The position coordinates of the nth EMVS are encapsulated in a vector $\boldsymbol{k}_n\in\mathbb{R}^3$, $n=1,\ldots,N$. The phase delays of the signals collected by different EMVSs can be represented by

the so-called spatial steering vector defined as follows:

$$\boldsymbol{a}_{\theta,\varphi} \triangleq \exp\left(\mathrm{i}2\pi\lambda^{-1}\left[\boldsymbol{k}_1{}^T\boldsymbol{v}_{(\theta,\varphi)},\ldots,\boldsymbol{k}_N{}^T\boldsymbol{v}_{(\theta,\varphi)}\right]^T\right), \quad (4)$$

where λ is the wavelength of the impinging signal. Therefore, the EMVS array response to a single impinging signal with DOA-polarization parameters $(\theta, \varphi, \gamma, \eta)$ can be written as:

$$\boldsymbol{\mathcal{X}}_{(\theta,\varphi,\gamma,\eta)}(n,k,t) = \boldsymbol{a}_{(\theta,\varphi)}(n)\cdot\boldsymbol{b}_{(\theta,\varphi,\gamma,\eta)}(k)\cdot\boldsymbol{s}(t), \quad (5)$$

where $\boldsymbol{s} \in \mathbb{C}^T$ is the source vector containing the complex envelop collected at T time samples. It is shown in (5) that the response of the EMVS array to a single source signal is a third-order rank-1 tensor of size $N \times K \times T$: $\boldsymbol{\mathcal{X}}_{(\theta,\varphi,\gamma,\eta)} = \boldsymbol{a}_{(\theta,\varphi)} \otimes \boldsymbol{b}_{(\theta,\varphi,\gamma,\eta)} \otimes \boldsymbol{s}$. In case where there are R incident signals, we denote $\boldsymbol{\mathcal{X}}_r = \boldsymbol{\mathcal{X}}_{(\theta_r,\varphi_r,\gamma_r,\eta_r)}$, $\boldsymbol{a}_r = \boldsymbol{a}_{(\theta_r,\varphi_r)}$, $\boldsymbol{b}_r = \boldsymbol{b}_{(\theta_r,\varphi_r,\gamma_r,\eta_r)}$, and $\boldsymbol{s}_r$ as the rth source vector. Then the EMVS array output can be written as:

$$\begin{aligned}\boldsymbol{\mathcal{X}} &= \sum_r^R \boldsymbol{\mathcal{X}}_r + \boldsymbol{\mathcal{N}} = \sum_r^R \boldsymbol{a}_r \otimes \boldsymbol{b}_r \otimes \boldsymbol{s}_r + \boldsymbol{\mathcal{N}} \\ &= [[\boldsymbol{A},\boldsymbol{B},\boldsymbol{S}]]_R + \boldsymbol{\mathcal{N}} \end{aligned} \quad (6)$$

where $\boldsymbol{A} \triangleq [\boldsymbol{a}_1,\ldots,\boldsymbol{a}_R]$, $\boldsymbol{B} \triangleq [\boldsymbol{b}_1,\ldots,\boldsymbol{b}_R]$, $\boldsymbol{S} \triangleq [\boldsymbol{s}_1,\ldots,\boldsymbol{s}_R]$ denotes the spatial steering matrix, the angular-polarization steering matrix, and the source signal matrix, respectively, and $\boldsymbol{\mathcal{N}}$ denote the noise term. For convenience, we will omit the noise term in following texts. Therefore, (6) can be abbreviated as:

$$\boldsymbol{\mathcal{X}} = \sum_r^R \boldsymbol{\mathcal{X}}_r = \sum_r^R \boldsymbol{a}_r \otimes \boldsymbol{b}_r \otimes \boldsymbol{s}_r = [\![\boldsymbol{A},\boldsymbol{B},\boldsymbol{S}]\!]_R, \quad (7)$$

It is shown in (7) that the EMVS array signal admits a CPD. We give the matrix representation of (7) as follows:

$$\boldsymbol{X} = (\boldsymbol{A}\odot\boldsymbol{B})\,\boldsymbol{S}^T, \quad (8)$$

where $\boldsymbol{X}$ denotes matrix representation of tensor $\boldsymbol{\mathcal{X}}$.

B. PROBLEM FORMULATION

Our goal is to estimate the DOA and polarization parameters from the observed signal $\boldsymbol{\mathcal{X}}$, as model in (6). This can be done via a CPD based approach. Briefly speaking, we first identify the factor matrices $\boldsymbol{A}$ and $\boldsymbol{B}$ by computing the CPD of $\boldsymbol{\mathcal{X}}$, and then calculate DOA and polarization parameters from the estimates of $\boldsymbol{A}$ and $\boldsymbol{B}$.

In this paper, we consider the scenarios where the source signals are fully or partially CM signals, and we incorporate this prior knowledge as a constraint into the CPD decomposition. More specifically, we consider the following two cases:

1) ALL SOURCES ARE CM SIGNALS (FULL CM CONSTRAINT)

In this case, we formulate the problem as CPD with CM constraint:

$$\begin{aligned}\left\{\tilde{\boldsymbol{A}},\tilde{\boldsymbol{B}},\tilde{\boldsymbol{S}}\right\} &= \underset{\{\boldsymbol{A},\boldsymbol{B},\boldsymbol{S}\}}{\arg\min}\left\|\boldsymbol{X}-(\boldsymbol{A}\odot\boldsymbol{B})\,\boldsymbol{S}^T\right\|_F^2, \\ &\quad s.t.\ \left|s_{t,r}\right| = c, \quad r=1,\cdots,R,\ t=1,\cdots,T,\end{aligned} \quad (9)$$

where c denotes the modulus of the source signals.

2) PART OF SOURCES ARE CM SIGNALS (PARTIAL CM CONSTRAINT)

Without loss of generality, we assume that the first R_1 sources are CM sources and that the remaining sources are orthogonal to the CM sources. In general, this implies that the non-CM signal sources are statistically uncorrelated with the CM signal sources. In this case, we aim to compute a CPD with partial CM constraint and orthogonality between CM and non-CM signals :

$$\begin{aligned}\left\{\tilde{\boldsymbol{A}},\tilde{\boldsymbol{B}},\tilde{\boldsymbol{S}}\right\} &= \underset{\{\boldsymbol{A},\boldsymbol{B},\boldsymbol{S}\}}{\arg\min}\left\|\boldsymbol{X}-(\boldsymbol{A}\odot\boldsymbol{B})\,\boldsymbol{S}^T\right\|_F^2, \\ &\quad s.t.\ \left\|s_{t,r}\right\| = c \quad \text{and } \boldsymbol{s}_r^H\cdot\boldsymbol{s}_{r'} = \boldsymbol{0}, \\ &\quad r\in[1,R_1], \quad r'\in[R_1+1,R], \\ &\quad t\in[1,T],\ R_1 < R.\end{aligned} \quad (10)$$

Optimization based algorithms (e.g., the Quasi-Newton algorithm) for computing the above constrained CPDs can be conveniently implemented via the framework of SDF, embedded in Tensorlab 3.0 [28], where the CM constraint is incorporated as a regularization term. However, there is no guarantee that the obtained source matrix has the CM property. In [32], an algebraic algorithm is proposed that combines the CPD structure and the CM constraint. However, the uniqueness conditions remain the same as those for unconstrained CPD, i.e., the CM constraint does not relax the working conditions for the algorithm. Therefore, in this paper, we will introduce two algebraic CPD algorithms with full and partial CM constraint, respectively, of which the uniqueness conditions are more relaxed than those of unconstrained CPD. The algorithms mainly make use of the well-known analytical constant modulus algorithm (ACMA) method and the inherent rank-1 structure of the matrix representation of each column of $(\boldsymbol{A}\odot\boldsymbol{B})$. To facilitate the use of ACMA, we have the following additional assumptions:

(A1) $(\boldsymbol{A}\odot\boldsymbol{B})$ has full column rank;

(A2) The CM sources are linearly independent and have sufficient phase variations. e.g., ACMA does not work for BPSK signals as they only have two different phases [30].

III. PROPOSED ALGORITHM

A. REVIEW OF ACMA

We first give a brief summary of the ACMA method. For more details, the reader is referred to [30]. We consider the following signal model:

$$\boldsymbol{Y} = \boldsymbol{M}\boldsymbol{S}^T, \quad (11)$$

where $\boldsymbol{Y} \in \mathbb{C}^{M\times T}$, $\boldsymbol{M} \in \mathbb{C}^{M\times R}$, and $\boldsymbol{S} \in \mathbb{C}^{T\times R}$ denote the observe signal, the mixing matrix, and the source matrix, respectively. We assume that $\boldsymbol{S}$ has CM property.

The key steps of ACMA are as follows:

(*i*) *Estimate in the row space of* $\boldsymbol{Y}$ *a set of basis vectors,* $\{\boldsymbol{v}_1,\cdots,\boldsymbol{v}_R\}$, *of the vector space spanned by the columns of* $\boldsymbol{S}$.

(*ii*) *Construct matrix* $\hat{\boldsymbol{P}} \in \mathbb{C}^{(T-1)\times R^2}$, *such that the basis vectors in* $\ker\left(\hat{\boldsymbol{P}}\right)$, $\{\boldsymbol{z}_1,\cdots,\boldsymbol{z}_R\}$ *can be reshaped into*

a third-order tensor that admits an overdetermined CPD. This mainly consists of the following sub-steps:

– Denote $\boldsymbol{V} \triangleq \{\boldsymbol{v}_1, \cdots, \boldsymbol{v}_R\}$, and $\boldsymbol{u}_t \triangleq \boldsymbol{V}(t,:)^T$. Construct $\boldsymbol{P}_t = \boldsymbol{u}_t \boldsymbol{u}_t^H, t = 1, \cdots, T$. Due to the CM constraint, we have $\boldsymbol{w}_r^T \boldsymbol{P}_t \boldsymbol{w}_r^* = c$, where $\boldsymbol{w}_r$ denotes a demixing vector such that $\boldsymbol{s}_r = \boldsymbol{V}\boldsymbol{w}_r$.

– Stack the vector representation of $\boldsymbol{P}_t$, $\boldsymbol{p}_t \triangleq \text{vec}(\boldsymbol{P}_t)$, into the columns of a matrix $\boldsymbol{P}$ of size $R^2 \times T$, which admits the following:

$$\boldsymbol{P}^T \boldsymbol{z}_r = \begin{bmatrix} c \\ \vdots \\ c \end{bmatrix}, \quad \text{where} \quad \boldsymbol{z}_r = \boldsymbol{w}_r \otimes \boldsymbol{w}_r^*.$$

– Construct a matrix $\hat{\boldsymbol{P}}$ of size $(T-1) \times R^2$ via the Householder transformation of $\boldsymbol{P}$:

$$\begin{bmatrix} \partial \\ \hat{\boldsymbol{P}} \end{bmatrix} = \boldsymbol{Q}\boldsymbol{P}^T,$$

i.e., $\hat{\boldsymbol{P}}$ contains the second to the last rows of $\boldsymbol{Q}\boldsymbol{P}^T$, where $\boldsymbol{Q}$ is a Householder transformation matrix. Due to assumption (A2), we have $\dim\left(\ker\left(\hat{\boldsymbol{P}}\right)\right) = R$.

– Calculate a set of R basis vectors of $\ker\left(\hat{\boldsymbol{P}}\right)$ $\{\boldsymbol{z}_1, \cdots, \boldsymbol{z}_R\}$ and obtain a tensor $\boldsymbol{\mathcal{Z}}$ from those vectors, which admits an overdetermined CPD:

$$\boldsymbol{\mathcal{Z}} \triangleq \text{Ten}\left([\boldsymbol{z}_1, \cdots, \boldsymbol{z}_R], R, R, R\right) = \left[\left[\boldsymbol{W}, \boldsymbol{W}^*, \boldsymbol{F}\right]\right]_R, \quad (12)$$

where $\boldsymbol{W} \triangleq [\boldsymbol{w}_1, \cdots \boldsymbol{w}_R]^T \in \mathbb{C}^{R \times R}$ denotes the demixing matrix, $\boldsymbol{F} \in \mathbb{C}^{R \times R}$ with $\boldsymbol{F}(k,l) = \lambda_{k,l}$, where $\lambda_{k,l}$ is the coefficient in equation (16) of [30].

(*iii*) *Compute the overdetermined CPD* (12) *to obtain* $\boldsymbol{W}$.

As the CPD $\boldsymbol{\mathcal{Z}} = \left[\left[\boldsymbol{W}, \boldsymbol{W}^*, \boldsymbol{F}\right]\right]_R$ is overdetermined, it can be computed algebraically via generalized eigenvalue decomposition (GEVD) [33], which makes use of two frontal slices of $\boldsymbol{\mathcal{Z}}$. We can also compute it via matrix simultaneous diagonalization (SD) that makes use of all the frontal slices. Once $\boldsymbol{W}$ has been computed, we immediately obtain $\boldsymbol{S}^T = \boldsymbol{W}\boldsymbol{Y}$.

In the above steps, we mainly consider the case where all the sources are CM signals. We note that, with similar steps, ACMA also applies in the case where part of the sources are CM signals. In this case, the algorithm only extracts the CM sources.

B. ALGEBRAIC CPD WITH FULL CM CONSTRAINT

Now we propose an algebraic algorithm for computing the constrained CPD (8). The algorithm consist of the following two steps:

1) IDENTIFY THE CM SOURCE SIGNALS VIA ACMA

By denoting $\boldsymbol{M} \triangleq \boldsymbol{A} \odot \boldsymbol{B}$, we can rewrite (8) as $\boldsymbol{X} = \boldsymbol{M}\boldsymbol{S}^T$. According to assumption (A1), we know that $\boldsymbol{M}$ has full column rank. Therefore, we can use ACMA to estimate the CM source matrix, $\tilde{\boldsymbol{S}}$.

2) CALCULATE FACTOR MATRICES $\tilde{\boldsymbol{A}}$ AND $\tilde{\boldsymbol{B}}$ VIA RANK-1 APPROXIMATION

Now that we have obtained one factor matrix $\tilde{\boldsymbol{S}}$, the other factor matrices of the CPD (6), $\tilde{\boldsymbol{A}}$ and $\tilde{\boldsymbol{B}}$, can be computed by exploiting the Kronecker-product structure of each column of the matricized columns of [34]:

$$\tilde{\boldsymbol{A}} \odot \tilde{\boldsymbol{B}} = \boldsymbol{X}\left(\tilde{\boldsymbol{S}}^T\right)^{\dagger}. \quad (13)$$

Indeed, in the noiseless case, each column of $\tilde{\boldsymbol{M}} = \tilde{\boldsymbol{A}} \odot \tilde{\boldsymbol{B}}$ is a vectorized rank-1 matrix:

$$\text{unvec}(\tilde{\boldsymbol{m}}_r) = \tilde{\boldsymbol{a}}_r \tilde{\boldsymbol{b}}_r^T, \quad r = 1, \cdots, R. \quad (14)$$

In the noisy case, (14) holds approximately, and $\tilde{\boldsymbol{a}}_r$ and $\tilde{\boldsymbol{b}}_r$ can be computed via the rank-1 approximation of unvec $(\tilde{\boldsymbol{m}}_r)$, which is usually done via singular value decomposition (SVD).

C. ALGEBRAIC CPD WITH PARTIAL CM CONSTRAINT

Now we propose an algebraic algorithm for computing the CPD with partial CM constraint and orthogonality between CM and non-CM sources.

We denote the CM part and the non-CM part of the source signals $\boldsymbol{S}$ as $\boldsymbol{S}_1 \in \mathbb{C}^{T \times R_1}$ and $\boldsymbol{S}_2 \in \mathbb{C}^{T \times R_2}$, respectively, where $R_1 + R_2 = R$. Analogously, we denote $\boldsymbol{A}_1 \in \mathbb{C}^{N \times R_1}$ and $\boldsymbol{A}_2 \in \mathbb{C}^{N \times R_2}$ as the submatrices that hold the first R_1 and the last R_2 columns of $\boldsymbol{A}$, respectively. Matrices $\boldsymbol{B}_1 \in \mathbb{C}^{K \times R_1}$ and $\boldsymbol{B}_2 \in \mathbb{C}^{K \times R_2}$ can be defined similarly. By definition, we know that $\boldsymbol{A}_1$ and $\boldsymbol{B}_1$ are associated with the CM part $\boldsymbol{S}_1$, and that $\boldsymbol{A}_2$ and $\boldsymbol{B}_2$ are associated with the non-CM part $\boldsymbol{S}_2$. Therefore, the observed signal $\boldsymbol{\mathcal{X}}$ can be expressed as: $\boldsymbol{\mathcal{X}} = \boldsymbol{\mathcal{X}}_1 + \boldsymbol{\mathcal{X}}_2$, where $\boldsymbol{\mathcal{X}}_1$ and $\boldsymbol{\mathcal{X}}_2$ admit a CPD separately: $\boldsymbol{\mathcal{X}}_1 = [\![\boldsymbol{A}_1, \boldsymbol{B}_1, \boldsymbol{S}_1]\!]_{R_1}$, $\boldsymbol{\mathcal{X}}_2 = [\![\boldsymbol{A}_2, \boldsymbol{B}_2, \boldsymbol{S}_2]\!]_{R_2}$.

1) IDENTIFY THE CM PART $\tilde{\boldsymbol{A}}_1$, $\tilde{\boldsymbol{B}}_1$ AND $\tilde{\boldsymbol{S}}_1$

We denote the matrix representation of $\boldsymbol{\mathcal{X}}_1$ and $\boldsymbol{\mathcal{X}}_2$ as $\boldsymbol{X}_1 = (\boldsymbol{A}_1 \odot \boldsymbol{B}_1)\boldsymbol{S}_1^T$ and $\boldsymbol{X}_2 = (\boldsymbol{A}_2 \odot \boldsymbol{B}_2)\boldsymbol{S}_2^T$, respectively, and $\boldsymbol{M}_1 \triangleq \boldsymbol{A}_1 \odot \boldsymbol{B}_1$, $\boldsymbol{M}_2 \triangleq \boldsymbol{A}_2 \odot \boldsymbol{B}_2$. Then we can further rewrite (6) as:

$$\boldsymbol{X} = \boldsymbol{M}_1 \boldsymbol{S}_1^T + \boldsymbol{M}_2 \boldsymbol{S}_2^T. \quad (15)$$

The mixing matrix $\boldsymbol{M} = [\boldsymbol{M}_1, \boldsymbol{M}_2]$ has full column rank under the assumption (A1). Therefore, we can use ACMA to identify the CM source signals $\tilde{\boldsymbol{S}}_1$.

We multiply both sides of (15) to the right by $\tilde{\boldsymbol{S}}_1^*$. Then, due to the orthogonality between $\tilde{\boldsymbol{S}}_1$ and $\tilde{\boldsymbol{S}}_2$, we have the following result:

$$\boldsymbol{X}\tilde{\boldsymbol{S}}_1 = \boldsymbol{M}_1 \boldsymbol{S}_1^T \tilde{\boldsymbol{S}}_1^* + \boldsymbol{M}_2 \boldsymbol{S}_2^T \tilde{\boldsymbol{S}}_1^* = \boldsymbol{M}_1 \boldsymbol{S}_1^T \tilde{\boldsymbol{S}}_1^*. \quad (16)$$

Note that $\tilde{\boldsymbol{S}}_1$ is already obtained, we can calculate $\tilde{\boldsymbol{M}}_1$ from (16): $\tilde{\boldsymbol{M}}_1 = \boldsymbol{X}\boldsymbol{S}_1\left(\tilde{\boldsymbol{S}}_1^T \tilde{\boldsymbol{S}}_1^*\right)^{\dagger}$. Then $\tilde{\boldsymbol{A}}_1$ and $\tilde{\boldsymbol{B}}_1$ can be calculated by rank-1 approximation of the matricized columns of: $\tilde{\boldsymbol{M}}_1 = \tilde{\boldsymbol{A}}_1 \odot \tilde{\boldsymbol{B}}_1$.

2) CALCULATE $\tilde{A}_2$, $\tilde{B}_2$ AND $\tilde{S}_2$ VIA CPD

Now that we have obtained $\tilde{\boldsymbol{A}}_1$, $\tilde{\boldsymbol{B}}_1$ and $\tilde{\boldsymbol{S}}_1$, we have $\tilde{\boldsymbol{\mathcal{X}}}_1 = [\![\tilde{\boldsymbol{A}}_1, \tilde{\boldsymbol{B}}_1, \tilde{\boldsymbol{S}}_1]\!]$. The non-CM part $\tilde{\boldsymbol{\mathcal{X}}}_2$ can be obtained as:

$$\tilde{\boldsymbol{\mathcal{X}}}_2 = \boldsymbol{\mathcal{X}} - \tilde{\boldsymbol{\mathcal{X}}}_1 = [\![\tilde{\boldsymbol{A}}_2, \tilde{\boldsymbol{B}}_2, \tilde{\boldsymbol{S}}_2]\!]_{R_2}. \tag{17}$$

As long as the uniqueness conditions hold for the unconstrained CPD (17), we can calculate $\tilde{\boldsymbol{A}}_2$, $\tilde{\boldsymbol{B}}_2$ and $\tilde{\boldsymbol{S}}_2$ by computing the unconstraint CPD of $\tilde{\boldsymbol{\mathcal{X}}}_2$.

We would like to mention that the two proposed algorithms are (semi-) algebraic, in the sense that they rely only on arithmetic operations, overdetermined sets of linear equations, matrix SVD or joint diagonalization, and GEVD. As no numerical optimization is involved, in which the cost function may have multiple local optima, it is shown through simulations that these algorithms have stable performance and low complexity, in comparison with optimization based algorithms. We also note that the proposed algorithms consist of several subproblems, which may have multiple solutions. E.g. the matrix joint diagonalization subproblem involved in ACMA and the unconstrained CPD subproblem in the second step of CPD-PCM-ALG have various solutions. Therefore, the overall complexity varies when we adopt different solutions to these subproblems. As such, in this paper, we do not formally analyze the complexity of the proposed algorithms.

D. DOA POLARIZATION ESTIMATION

Now we explain how to compute DOA and polarization parameters via the estimates $\tilde{\boldsymbol{A}}$ and $\tilde{\boldsymbol{B}}$. We first present the cross-product-based DOA and polarization estimator in the general case. Then we introduce a refinement scheme to further improve the estimation accuracy, in the particular case that the sensor spacing is larger than half wavelength of the impinging signal.

1) DOA-POLARIZATION ESTIMATION VIA CROSS-PRODUCT

For convenience, we assume that the tripole antenna is used such that the angular-polarization steering vector $\boldsymbol{b}_{\theta,\varphi,\gamma,\eta} = \boldsymbol{e}_{\theta,\varphi,\gamma,\eta}$. According to [35], we have the following result:

$$\boldsymbol{e}_{\theta,\varphi,\gamma,\eta} \wedge \boldsymbol{e}^*_{\theta,\varphi,\gamma,\eta} = 2\mathrm{i}\sin\eta\sin\gamma\cos\gamma\boldsymbol{v}_{(\theta,\varphi)}, \tag{18}$$

where the Poynting vector $\boldsymbol{v}_{(\theta,\varphi)}$ denotes the DOA of the impinging signal. We can also calculate the polarization parameters from $\boldsymbol{b}_{\theta,\varphi,\gamma,\eta}$. For instance, we first construct a vector:

$$\begin{aligned}\rho &= \left[\frac{e_x}{e_z}, \frac{e_y}{e_z}\right]^T = \left[\frac{b_x}{b_z}, \frac{b_y}{b_z}\right]^T \\ &= \begin{bmatrix} -\cot\varphi\cos\theta + \cot\gamma\dfrac{\sin\theta}{\sin\varphi}\cos\eta - \mathrm{i}\cot\gamma\dfrac{\sin\theta}{\sin\varphi}\sin\eta \\ -\cot\varphi\sin\theta - \cot\gamma\dfrac{\cos\theta}{\sin\varphi}\cos\eta + \mathrm{i}\cot\gamma\dfrac{\cos\theta}{\sin\varphi}\sin\eta \end{bmatrix}.\end{aligned} \tag{19}$$

Then (γ, η) can be computed as:

$$\begin{cases} \eta = -\angle(b_x\sin\theta - b_y\cos\theta) \\ \gamma = \operatorname{arccot}\left(\dfrac{\operatorname{im}\left(b_y\sin\varphi\right)}{\cos\theta\sin\eta}\right). \end{cases} \tag{20}$$

As such, for each column $\tilde{\boldsymbol{b}}_r$ of matrix $\tilde{\boldsymbol{B}}$, we can use cross-product (18) to obtain the DOA of each signal and use (19), (20) to obtain the polarization parameters of each signal.

Note that the above derivation is based on the tripole, which consists of three sensors. For EMVSs with four to six sensors, the above calculation also applies. For instance, if the EMVS has four or five sensors, we can apply the above formulas (18)–(20) to the submatrix that holds the first three rows of $\tilde{\boldsymbol{B}}$. If a complete EMVS is employed, i.e., it has six sensors, we can apply the cross-product based scheme between the electric field measurement and the magnetic field measurement to obtain the DOA. The polarization parameters can be obtained via (19) and (20).

The above cross-product based scheme is able to generate coarse yet unambiguous DOA and polarization estimates in the general case. However, it dose not make use of the spatial aperture of the EMVS array, in particular, a spatially sparse array with sensor spacing $d \gg \lambda/2$. Therefore, in order to further improve the DOA estimation accuracy, we can use a refinement scheme.

2) ESTIMATION REFINEMENT

We assume that the sensor spacing $d \gg \lambda/2$. For convenience, we limit our derivation to the case that an L-shaped array of three EMVSs is employed. In this case, we have $\boldsymbol{k}^{(1)} = [d, 0, 0]^T, \boldsymbol{k}^{(2)} = [0, 0, 0]^T$ and $\boldsymbol{k}^{(3)} = [0, d, 0]^T$. We assume that the spatial steering vector has been obtained via the proposed algorithms. We denote $[u, v, w] \triangleq \boldsymbol{v}_{(\theta,\varphi)}$, then the spatial steering vector (4) can be written as $\boldsymbol{a}_{(\theta,\varphi)} = \left[\exp\left(-\mathrm{i}2\pi d\lambda^{-1}u\right), 1, \exp\left(-\mathrm{i}2\pi d\lambda^{-1}v\right)\right]^T$. Then we have the following result after several simple derivations:

$$\begin{cases} u'_{m_1} = 0.5\lambda d^{-1}\pi^{-1}\angle\left\{\dfrac{\boldsymbol{a}(1)}{\boldsymbol{a}(2)}\right\} + \lambda d^{-1}m_1 \\ v'_{m_2} = 0.5\lambda d^{-1}\pi^{-1}\angle\left\{\dfrac{\boldsymbol{a}(3)}{\boldsymbol{a}(2)}\right\} + \lambda d^{-1}m_2. \end{cases} \tag{21}$$

Note that, as $d \gg \lambda/2$, (21) generates two sets of accurate yet ambiguous estimates u'_{m_1} and v'_{m_2}. The ambiguity is characterized by integers m_1 and m_2, which can be arbitrary. Here, we use the estimates obtained by the cross-product based scheme to remove this ambiguity. More precisely, we denote by u_{cp} and v_{cp} the estimates of u and v, obtained by the cross-product-based estimator, and then the optimal m_1, m_2 can be calculated by:

$$\begin{cases} \tilde{m}_1 = \arg\min\limits_{m_1}\left|u'_{m_1} - u_{cp}\right| \\ \tilde{m}_2 = \arg\min\limits_{m_2}\left|v'_{m_2} - v_{cp}\right|. \end{cases} \tag{22}$$

TABLE 1. Explicit expression of each entry of fisher information matrix.

$$\boldsymbol{J}_{\varphi,\varphi}=\frac{2N}{\sigma^2}\begin{pmatrix}\frac{4\pi^2}{\lambda^2}\left(\left(\boldsymbol{p}_2^T\boldsymbol{k}^{(1)}\right)^2+\left(\boldsymbol{p}_2^T\boldsymbol{k}^{(2)}\right)^2+\left(\boldsymbol{p}_2^T\boldsymbol{k}^{(3)}\right)^2\right)+3\sin^2\gamma\\ -\frac{8\pi^2}{\lambda^2}\sin\varphi\cos\gamma\sin\gamma\cos\eta\left(\left(\boldsymbol{p}_2^T\boldsymbol{k}^{(1)}\right)^2+\left(\boldsymbol{p}_2^T\boldsymbol{k}^{(2)}\right)^2+\left(\boldsymbol{p}_2^T\boldsymbol{k}^{(3)}\right)^2\right)\\ -\frac{8\pi}{\lambda^2}\sin^2\varphi\sin^2\gamma\sin^2\eta\left(\left(\boldsymbol{p}_2^T\boldsymbol{k}^{(1)}\right)^2+\left(\boldsymbol{p}_2^T\boldsymbol{k}^{(2)}\right)^2+\left(\boldsymbol{p}_2^T\boldsymbol{k}^{(3)}\right)^2\right)\\ +\frac{4\pi}{\lambda}\cos\gamma\sin\gamma\cos\varphi\sin\eta\left(\boldsymbol{p}_2^T\boldsymbol{k}^{(1)}+\boldsymbol{p}_2^T\boldsymbol{k}^{(2)}+\boldsymbol{p}_2^T\boldsymbol{k}^{(3)}\right)\end{pmatrix}$$

$$\boldsymbol{J}_{\theta,\theta}=\frac{2N}{\sigma^2}\begin{pmatrix}\frac{4\pi^2}{\lambda^2}\left(\cos^2\gamma\sin^2\gamma+\cos^2\gamma-2\cos\gamma\sin\gamma\sin\varphi\cos\eta+\sin^2\varphi\sin^2\gamma\right)\\ \left(\left(\boldsymbol{p}_1^T\boldsymbol{k}^{(1)}\right)^2+\left(\boldsymbol{p}_1^T\boldsymbol{k}^{(2)}\right)^2+\left(\boldsymbol{p}_1^T\boldsymbol{k}^{(3)}\right)^2\right)+3\cos^2\varphi\sin^2\gamma\end{pmatrix}$$

$$\boldsymbol{J}_{\gamma,\gamma}=\frac{2N}{\sigma^2}\left(3+3\sin 2\gamma\sin\varphi\cos\eta\right)$$

$$\boldsymbol{J}_{\eta,\eta}=\frac{2N}{\sigma^2}3\sin^2\gamma$$

$$\boldsymbol{J}_{\eta,\gamma}=\boldsymbol{J}_{\gamma,\eta}=-\frac{2N}{\sigma^2}\sin^2\gamma\sin\varphi\sin\eta$$

$$\boldsymbol{J}_{\theta,\varphi}=\boldsymbol{J}_{\varphi,\theta}=\frac{2N}{\sigma^2}\begin{pmatrix}\frac{4\pi^2}{\lambda^2}\left(\boldsymbol{p}_1^T\boldsymbol{k}^{(1)}\boldsymbol{p}_2^T\boldsymbol{k}^{(1)}+\boldsymbol{p}_1^T\boldsymbol{k}^{(2)}\boldsymbol{p}_2^T\boldsymbol{k}^{(2)}+\boldsymbol{p}_1^T\boldsymbol{k}^{(3)}\boldsymbol{p}_2^T\boldsymbol{k}^{(3)}\right)\\ -\frac{8\pi^2}{\lambda^2}\sin\varphi\cos\gamma\sin\gamma\cos\eta\\ \left(\boldsymbol{p}_1^T\boldsymbol{k}^{(1)}\boldsymbol{p}_2^T\boldsymbol{k}^{(1)}+\boldsymbol{p}_1^T\boldsymbol{k}^{(2)}\boldsymbol{p}_2^T\boldsymbol{k}^{(2)}+\boldsymbol{p}_1^T\boldsymbol{k}^{(3)}\boldsymbol{p}_2^T\boldsymbol{k}^{(3)}\right)\\ -\frac{8\pi}{\lambda^2}\sin^2\varphi\sin^2\gamma\sin^2\eta\\ \left(\boldsymbol{p}_1^T\boldsymbol{k}^{(1)}\boldsymbol{p}_2^T\boldsymbol{k}^{(1)}+\boldsymbol{p}_1^T\boldsymbol{k}^{(2)}\boldsymbol{p}_2^T\boldsymbol{k}^{(2)}+\boldsymbol{p}_1^T\boldsymbol{k}^{(3)}\boldsymbol{p}_2^T\boldsymbol{k}^{(3)}\right)\\ -\frac{2\pi}{\lambda}\cos\varphi\sin\gamma\cos\gamma\sin\eta\end{pmatrix}$$

$$\boldsymbol{J}_{\varphi,\gamma}=\boldsymbol{J}_{\gamma,\varphi}=\frac{2N}{\sigma^2}\begin{pmatrix}3\sin^2\gamma\cos\varphi\cos\eta+\frac{2\pi}{\lambda}\sin\varphi\sin\eta\left(\sin^2\gamma-\cos^2\gamma\right)\\ \left(\boldsymbol{p}_2^T\boldsymbol{k}^{(1)}+\boldsymbol{p}_2^T\boldsymbol{k}^{(2)}+\boldsymbol{p}_2^T\boldsymbol{k}^{(3)}\right)\end{pmatrix}$$

$$\boldsymbol{J}_{\theta,\gamma}=\boldsymbol{J}_{\gamma,\theta}=\frac{2N}{\sigma^2}\left(-\frac{2\pi}{\lambda}\sin\varphi\sin\eta\left(\boldsymbol{p}_1^T\boldsymbol{k}^{(1)}+\boldsymbol{p}_1^T\boldsymbol{k}^{(2)}+\boldsymbol{p}_1^T\boldsymbol{k}^{(3)}\right)\right)$$

$$\boldsymbol{J}_{\varphi,\eta}=\boldsymbol{J}_{\eta,\varphi}=\frac{2N}{\sigma^2}\frac{2\pi}{\lambda}\left(\sin^2\gamma-\sin\varphi\sin\gamma\cos\gamma\cos\eta\right)\left(\boldsymbol{p}_2^T\boldsymbol{k}^{(1)}+\boldsymbol{p}_2^T\boldsymbol{k}^{(2)}+\boldsymbol{p}_2^T\boldsymbol{k}^{(3)}\right)$$

$$\boldsymbol{J}_{\theta,\eta}=\boldsymbol{J}_{\eta,\theta}=\frac{2N}{\sigma^2}\begin{pmatrix}\frac{2\pi}{\lambda}\left(\sin^2\gamma-\cos\gamma\sin\gamma\sin\varphi\cos\eta\right)\\ \left(\boldsymbol{p}_1^T\boldsymbol{k}^{(1)}+\boldsymbol{p}_1^T\boldsymbol{k}^{(2)}+\boldsymbol{p}_1^T\boldsymbol{k}^{(3)}\right)\end{pmatrix}$$

The refined estimates $\tilde{u}$, $\tilde{v}$ are obtained by substituting $\tilde{m}_1$ and $\tilde{m}_2$ into (21). Once we obtain $\tilde{u}$ and $\tilde{v}$, we immediately obtain the DOA estimates $\left(\tilde{\theta},\tilde{\varphi}\right)$ by solving the equations $\tilde{u}=\cos\tilde{\theta}\sin\tilde{\varphi}$, $\tilde{v}=\sin\tilde{\theta}\sin\tilde{\varphi}$. The refined polarization parameter estimates can be further obtained via (20).

The above estimation refinement scheme is based on an L-shaped array of three EMVSs. In practice, the scheme may not be limited to L-shaped arrays. Similar derivations also apply to other types of array configuration, e.g., the circular array or square array. However, we note that if a uniform linear array is used, we may not be able to refine the two parameters, u and v, because we can only obtain one equation in the place of (21). In this case, the scheme refines either u or v. In addition, if more than three EMVSs are employed, we can choose three of them to constitute a subarray, for which the estimation refinement scheme may be applied. In general, we can let the constructed subarray be as large as possible, to make the best use of the spatial aperture of the EMVS array.

E. CRAMÉR-RAO BOUNDS

Here we derive the Cramér-Rao Bound (CRB) for DOA and polarization estimation based on an array of EMVS's, which may serve as a reference of accuracy for the proposed methods. We assume that a far-field narrowband signal with wavelength λ is impinging. Then the array output signal model can be written as:

$$\boldsymbol{x}(t)=\left(\boldsymbol{a}_{\theta,\varphi}\otimes\boldsymbol{b}_{\theta,\varphi,\gamma,\eta}\right)s(t)+\boldsymbol{n}(t) \tag{23}$$

where $\boldsymbol{n}(t)$ is white Gaussian noise with a priori known variance σ^2, $\boldsymbol{a}_{\theta,\varphi}$ is the spatial steering vector, and $\boldsymbol{b}_{\theta,\varphi,\gamma,\eta}$ is the angular-polarization steering vector, defined as (4) and (2) in Subsection II.A. We assume that the array signal is sampled at time instants $t_1\ldots,t_N$. Then the data-vector can be defined as:

$$\begin{aligned}\boldsymbol{z}&\triangleq\left[\boldsymbol{x}^T(t_1)\cdots\boldsymbol{x}^T(t_N)\right]^T\\&=\boldsymbol{a}_{\theta,\varphi}\otimes\boldsymbol{b}_{\theta,\varphi,\gamma,\eta}\otimes\boldsymbol{s}+\boldsymbol{\varepsilon}\end{aligned} \tag{24}$$

where $\boldsymbol{s}\triangleq[s(t_1),\ldots,s(t_N)]^T$, $\boldsymbol{\varepsilon}\triangleq[\boldsymbol{n}^T(t_1),\ldots,\boldsymbol{n}^T(t_N)]^T$ and N denotes the number of time samples. We let $\boldsymbol{\psi}\triangleq[\theta,\varphi,\gamma,\eta]^T$ be the vector of to-be-estimated parameters, and denote $\boldsymbol{\alpha}\triangleq\boldsymbol{a}_{\theta,\varphi}\otimes\boldsymbol{b}_{\theta,\varphi,\gamma,\eta}\otimes\boldsymbol{s}$, then we can obtain the Fisher Information Matrix (FIM) as follows:

$$\begin{aligned}\boldsymbol{J}_{k,l}&\triangleq 2Re\left[\frac{\partial\boldsymbol{\alpha}^H}{\partial\boldsymbol{\psi}_k}\boldsymbol{\Gamma}^{-1}\frac{\partial\boldsymbol{\alpha}}{\partial\boldsymbol{\psi}_l}\right]\\&=\frac{2N}{\sigma^2}Re\left[\frac{\partial\left(\boldsymbol{a}_{\theta,\varphi}\otimes\boldsymbol{b}_{\theta,\varphi,\gamma,\eta}\right)^H}{\partial\boldsymbol{\psi}_k}\frac{\partial\left(\boldsymbol{a}_{\theta,\varphi}\otimes\boldsymbol{b}_{\theta,\varphi,\gamma,\eta}\right)}{\partial\boldsymbol{\psi}_l}\right]\end{aligned} \tag{25}$$

where $k,l=1,2,3,4.$, $\boldsymbol{\Gamma}=\boldsymbol{\Gamma}_0\otimes\boldsymbol{I}_N$, $\boldsymbol{\Gamma}_0$ denotes the covariance matrix of the noise term $\boldsymbol{n}(t)$, $\boldsymbol{I}_N$ is a unit matrix. Then the CRB of $\boldsymbol{\psi}_k$can be calculated as follows:

$$CRB\left(\boldsymbol{\psi}_k\right)=\left(\boldsymbol{J}^{-1}\right)_{k,k},\quad k=1,2,3,4. \tag{26}$$

We have derived the explicit expression of each entry of $\boldsymbol{J}$ in the simple case where the array consists of three tripole antennas, which are summarized in TABLE 1 with $\boldsymbol{p}_1\triangleq[-\sin\theta\sin\varphi;\cos\theta\sin\varphi;0]$ and $\boldsymbol{p}_2\triangleq[\cos\theta\cos\varphi;\sin\theta\sin\varphi;-\sin\varphi]$.

F. DISCUSSION ON UNIQUENESS CONDITIONS

Here we discuss the generic uniqueness conditions for CPD with full CM (FCM) constraint and partial CM (PCM) constraint, respectively. For comparison, we first introduce the generic uniqueness conditions of an unconstrained CPD. In [36], it is shown that the CPD of an $N\times K\times T$ tensor of rank R is generic unique if the following conditions hold:

$$\begin{cases}R(R-1)\le NK(N-1)(K-1)/2\\ R\le T.\end{cases} \tag{27}$$

Note that the above uniqueness conditions are sufficient yet not necessary for unconstrained CPD, and that there have been more relaxed results in the literature. We refer the readers to [37] and [38] for details.

For CPD with full CM constraint, we note that the algebraic algorithm, as described in Subsection III-B, requires that the working assumptions (A1) and (A2) for ACMA hold, and that the factor matrix $\boldsymbol{S}$ has full column rank. Therefore, $\boldsymbol{A}\odot\boldsymbol{B}$ and

$\boldsymbol{S}$ need to have full column rank, and there should be sufficient phase variations in $\boldsymbol{S}$. Generically, a matrix has full column rank if it has more rows than columns. Therefore, the generic uniqueness conditions for CPD with full CM constraint are:

$$R \leq \min\left(NK, T\right). \tag{28}$$

For CPD with partial CM constraint, we note that the algebraic algorithm has two steps, as described in Section III-C. The first step uses ACMA, the orthogonality between the CM and non-CM parts, and the CPD structure to identify the CM part of the factor matrices, namely $\boldsymbol{A}_1$, $\boldsymbol{B}_1$, $\boldsymbol{S}_1$. Therefore, the working assumptions for this step are analogous to (28). The second step relies on an unconstrained CPD of the non-CM part $\boldsymbol{\mathcal{X}}_2$. Hence, the unconstrained CPD uniqueness conditions for $\boldsymbol{\mathcal{X}}_2$ need to be satisfied. As such, the generic uniqueness conditions for CPD with partial CM constraint are:

$$\begin{cases} R_2\left(R_2-1\right) \leq NK\left(N-1\right)\left(K-1\right)/2 \\ R_2 \leq T \\ R \leq NK. \end{cases} \tag{29}$$

Note that the uniqueness conditions for CPD with full and partial CM constraint are more relaxed than those for unconstrained CPD. To illustrate this, we list several typical values of $R_{\max}$ in TABLE 2. where $R_{\max}$ denotes the maximal number of R for which the decomposition can be unique. For clarity, we let $N = K$ for CPD, CPD-FCM and CPD-PCM. In addition, for CPD-PCM, we let $R_1 = \lfloor R/2 \rfloor$, where $\lfloor \cdot \rfloor$ rounds the number to the nearest integer less than or equal to that number.

TABLE 2. Generic value of $R_{\max}$ for CPD, CPD-FCM and CPD-PCM.

N	2	3	4	5	6	7	8
CPD	2	4	9	14	21	30	40
CPD-FCM	4	9	16	25	36	49	64
CPD-PCM	4	8	16	25	36	49	64

IV. SIMULATION RESULTS

In this section we present simulation results to demonstrate the performance of the proposed algebraic algorithms for CPD-FCM and CPD-PCM, in comparison with the corresponding optimization based algorithms, and unconstrained CPD. In simulation A, we show the performance of the compared algorithms in the case where all the sources are CM signals. In simulation B, we mainly show the performance of the compared algorithms in the case where only part of the sources are CM signals.

We use the following abbreviations:

– CPD-FCM-ALG: proposed algebraic CPD-FCM method.

– CPD-PCM-ALG: proposed algebraic CPD-PCM method.

– CPD-FCM-QN (ALG): quasi-Newton CPD-FCM method, initialized with the result of CPD-FCM-ALG.

– CPD-FCM-QN (RAND): quasi-Newton CPD-FCM method with random initialization.

– CPD-PCM-QN (ALG): quasi-Newton CPD-PCM method, initialized with the result of CPD-PCM-ALG.

– CPD-PCM-QN (RAND): quasi-Newton CPD-PCM method with random initialization.

– CPD: unconstrained canonical polyadic decomposition, initialized with algebraic CPD.

– ESPRIT: estimation of signal parameter via rotational invariance techniques, it is a method based on matrix eigenspace decomposition.

– MUSIC: multiple signal classification, it is a method based on matrix eigenspace decomposition.

Note that the tensor based approach proposed in [**?**] corresponds to the unconstrained CPD method.We implement CPD-FCM-QN (ALG), CPD-FCM-QN (RAND), CPD-PCM-QN (ALG) and CPD-PCM-QN (RAND) with the '*sdf_minf*' function [28], where the CM constraint is incorporated as a regularization term via the use of domain specific language. The tolerance on the relative function value, relative step size and maximum number iterations for '*sdf_minf*' are set to $TolFun = 10^{-10}$, $TolX = 10^{-8}$ and $MaxIter = 2000$, respectively. For CPD-FCM-QN (RAND) and CPD-PCM-QN (RAND), we try ten random initial values and select the one that gives the best fit after the first ten iterations to effectively initialize the algorithm. For all above algorithms, the weight of the regularization term is set to $RelWeight = 10^{-3}$. In the implementation of CPD, the tolerance on the relative function value and relative step size in the stopping criteria of '*cpd_nls*' [28] are set to $TolFun = 10^{-12}$ and $TolX = 10^{-8}$, respectively.

We assume that R far-field, narrowband signals with identical carrying frequency are impinging upon an L-shaped array of triple antennas. The spacing between adjacent antennas is $d = 6\lambda$. The number of snapshots is set to $T = 1000$. Therefore, the array output signals is a third-order tensor $\boldsymbol{\mathcal{X}}$ of size $3 \times 3 \times 1000$, admitting a CPD of rank R. In simulations, we mainly consider the case $R > 3$. In this case, the first two dimensions of $\boldsymbol{\mathcal{X}}$ are smaller than R, and CPD is usually labelled as ''underdetermined''. In addition, the noise term is generated as white Gaussian noise. The signal-to-noise ratio (SNR) is defined as follows:

$$SNR \triangleq 20\log_{10}\left(P_s/P_n\right). \tag{30}$$

where P_s and P_n denote the signal and noise levels, respectively. We use the *Root Mean Squared Error* (*RMSE*) to measure the accuracy of DOA and polarization estimation for each signal, which is defined as follows:

$$RMSE = \sqrt{\sum_{m=1}^{M} \frac{\left(\tilde{\alpha}_m - \alpha\right)^2}{M}}, \tag{31}$$

where $\alpha \in \{\theta, \varphi, \gamma, \eta\}$ denotes one of the to-be-estimated parameters, $\tilde{\alpha}_m$ denotes the estimate of α in the mth Monte Carlo experiment, and M denotes the number of Monte Carlo runs, which is set to $M = 200$ in all simulations. For the

evaluation of the overall accuracy, we further use the Overall *RMSE*, which is defined as the mean *RMSE* values of all the signals.

The simulations are performed on a workstation with the following configuration, CPU: Intel Xeon E5-2640 v4 @ 2.4 GHz; Memory: 128GB; System: 64bit Windows 10; MATLABR2016a.

A. RESULTS UNDER FULL CM CONSTRAINT

We first consider DOA and polarization estimation under full CM constraint in the overdetermined case. We conduct three simulations to show the performance of the proposed methods. In the first simulation, we testify the effectiveness of the proposed CPD-FCM-ALG method against CRB as a benchmark. We fix the number of snapshots to $T = 1000$ and let SNR vary between 0dB and 100dB, the results are given in FIGURE 3.Then, we fix SNR to 20dB and let T vary between 200 and 1000, the results are given in FIGURE 4. We can see that with the increase of SNR or the number of snapshots, the accuracy of CPD-FCM-ALG approaches CRB.

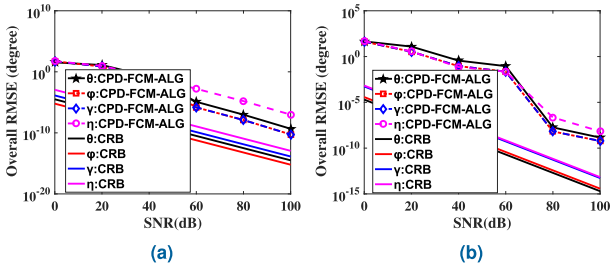

FIGURE 3. Overall RMSE and CRB versus SNR in the overdetermined case with full CM constraint: $N = K = 3$, $R = 2$, $T = 1000$. (a) Results with the first source. (b) Results with the second source.

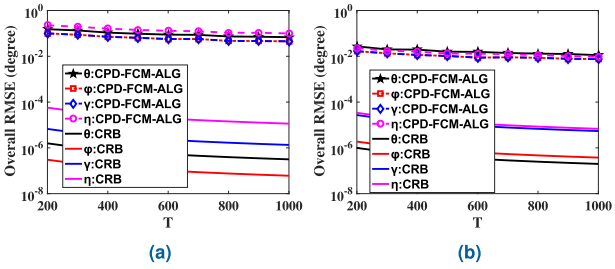

FIGURE 4. Overall RMSE and CRB versus T in the overdetermined case with full CM constraint: $N = K = 3$, $R = 2$, $SNR = 20$dB. (a) Results with the first source. (b) Results with the second source.

In the next two simulations, we compare CPD-FCM-ALG, CPD-FCM-QN(ALG), CPD-FCM-QN(Rand) with MUSIC, ESPRIT and CPD. In the second simulation we fix the number of snapshots to 1000 and let SNR vary between 0dB and 10dB. We assume that there are $R = 2$ impinging signals. The DOA-polarization parameters of the two signals are $(\theta_1, \varphi_1, \gamma_1, \eta_1) = (20°, 10°, 15°, 25°)$, $(\theta_2, \varphi_2, \gamma_2, \eta_2) = (60°, 40°, 45°, 70°)$, respectively. In the third simulation, we fix SNR to 10dB and let the number of snapshots vary between 40 and 200.

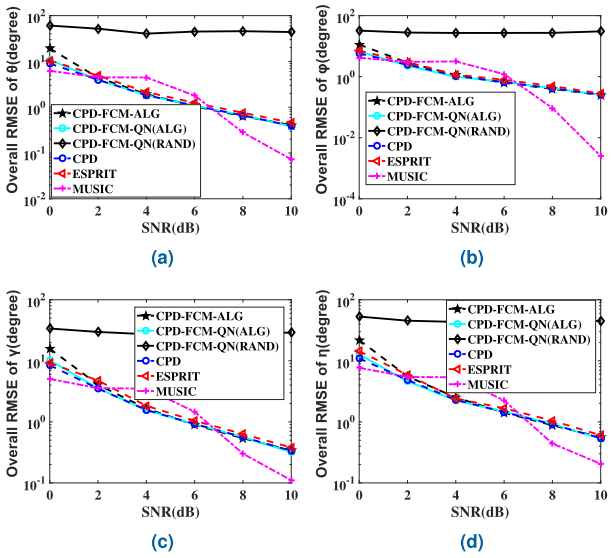

FIGURE 5. Overall RMSE of θ, φ, γ and η versus SNR in the overdetermined case with full CM constraint: $N = K = 3$, $R = 2$, $T = 1000$. It shows that the proposed method has almost identical performance as unconstrained CPD. MUSIC has best performance when there are sufficiently large number of snapshots and high SNR. (a) Overall RMSE of θ. (b) Overall RMSE of φ. (c) Overall RMSE of γ. (d) Overall RMSE of η.

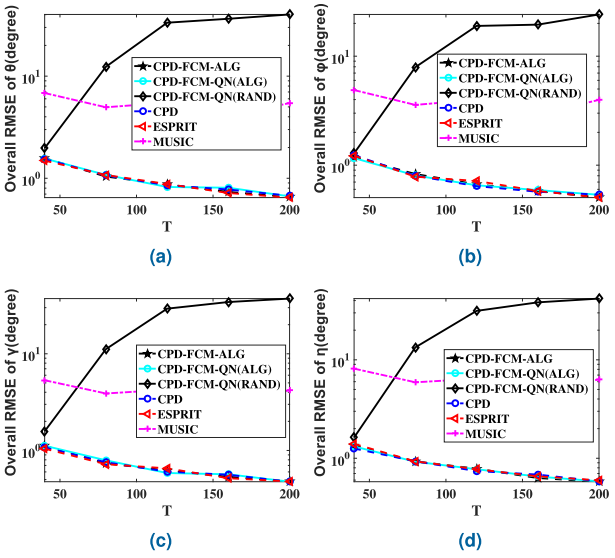

FIGURE 6. Overall RMSE of θ, φ, γ and η versus T in the overdetermined case with full CM constraint: $N = K = 3$, $R = 2$, $SNR = 10dB$. It shows that the proposed method has almost identical performance as unconstrained CPD, which is slightly better than that of ESPRIT. However, when the number of snapshots is small, MUSIC does not perform as well as other methods. (a) Overall RMSE of θ. (b) Overall RMSE of φ. (c) Overall RMSE of γ. (d) Overall RMSE of η.

The DOA-polarization parameters of the two signals are $(\theta_1, \varphi_1, \gamma_1, \eta_1) = (22.5°, 22.5°, 22.5°, 22.5°)$, $(\theta_2, \varphi_2, \gamma_2, \eta_2) = (112.5°, 67.5°, 67.5°, 67.5°)$, respectively.

The Overall RMSE curves in the above two simulations are plotted in FIGURE 5 and FIGURE 6, respectively. We can see that in the overdetermined case CPD-FCM-ALG, CPD-FCM-QN(ALG), and CPD have almost identical

performance, which is slightly better than that of ESPRIT. MUSIC has the best performance when there are sufficiently large number of snapshots and high SNR. However, when the number of snapshots is small, MUSIC does not perform as well as other methods. This can be explained as follows: the performance of MUSIC mainly relies on how accurate the noise subspace can be estimated, while the noise subspace is usually calculated via the eigenvalue decomposition(EVD) of the covariance matrix of the array signal. When the number of snapshots is small, the covariance matrix may be poorly estimated due to finite sampling effect, which leads to inaccurate estimation of noisespace and poor performance of the algorithm. In addition, we see that CPD-FCM-QN(Rand) only works when the number of snapshots is small. This is because in this method, the CM property is exploited as a soft constraint (or as a regularization term), which only works when the number of snapshots is small.

Next, we consider DOA and polarization estimation under full CM constraint in the underdetermined case. In this case, MUSIC and ESPRIT are not included in the comparison. We mainly consider the following two settings: (*i*) a highly underdetermined case $R = 6$; (*ii*) an extremely underdetermined case $R = 8$. The corresponding parameter settings are listed in TABLE 3 and TABLE 4, respectively.

TABLE 3. Simulation setting of DOA and polarization parameters in the highly underdetermined case: $N = K = 3$, $R = 6$.

	θ	φ	γ	η
#1	$\pi/24$	$\pi/24$	$\pi/24$	$\pi/24$
#2	$3\pi/8$	$\pi/8$	$\pi/8$	$\pi/8$
#3	$17\pi/24$	$5\pi/24$	$5\pi/24$	$5\pi/24$
#4	$25\pi/24$	$7\pi/24$	$7\pi/24$	$7\pi/24$
#5	$11\pi/6$	$3\pi/8$	$3\pi/8$	$3\pi/8$
#6	$41\pi/24$	$11\pi/24$	$11\pi/24$	$11\pi/24$

TABLE 4. Simulation setting of DOA and polarization parameters in the extremely underdetermined case: $N = K = 3$, $R = 8$.

	θ	φ	γ	η
#1	$\pi/32$	$\pi/32$	$\pi/32$	$\pi/32$
#2	$391\pi/1440$	$3\pi/32$	$3\pi/32$	$3\pi/32$
#3	$47\pi/96$	$5\pi/32$	$5\pi/32$	$5\pi/32$
#4	$23\pi/32$	$7\pi/32$	$7\pi/32$	$7\pi/32$
#5	$91\pi/96$	$9\pi/32$	$9\pi/32$	$9\pi/32$
#6	$113\pi/96$	$11\pi/32$	$11\pi/32$	$11\pi/32$
#7	$45\pi/32$	$13\pi/32$	$13\pi/32$	$13\pi/32$
#8	$157\pi/96$	$15\pi/32$	$15\pi/32$	$15\pi/32$

We let SNR vary from 0 dB to 40 dB. The Overall RMSE curves versus SNR for the above two settings are plotted in FIGURE 7 and FIGURE 8, respectively.

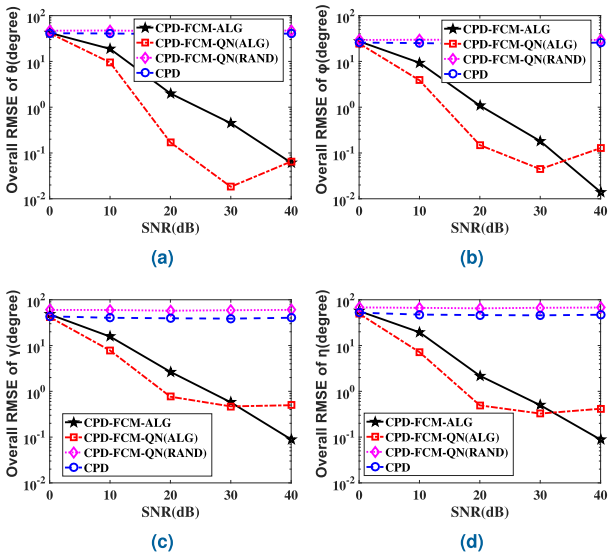

FIGURE 7. Overall RMSE of θ, φ, γ and η versus SNR in the highly underdetermined case with full CM constraint: $N = K = 3$, $R = 6$, $T = 1000$. It shows that only CPD-FCM-ALG and CPD-FCM-QN (ALG) yield accurate estimates at medium and high SNR levels. (a) Overall RMSE of θ. (b) Overall RMSE of φ. (c) Overall RMSE of γ. (d) Overall RMSE of η.

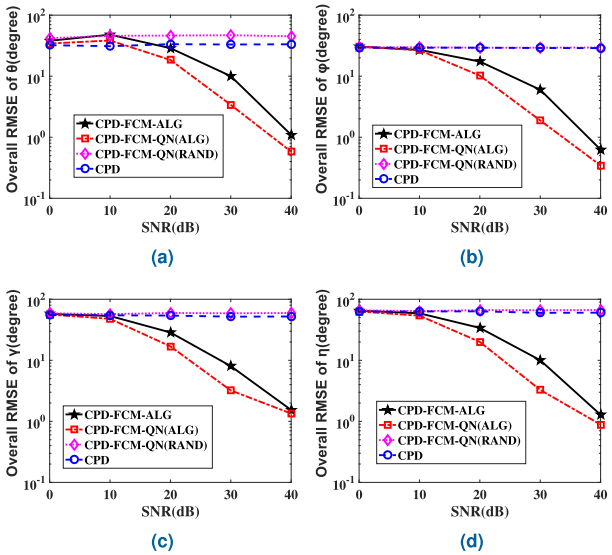

FIGURE 8. Overall RMSE of θ, φ, γ and η versus SNR in the extremely underdetermined case with full CM constraint: $N = K = 3$,$R = 8$, $T = 1000$. It shows that only CPD-FCM-ALG and CPD-FCM-QN (ALG) yield accurate estimates at high SNR levels. (a) Overall RMSE of θ. (b) Overall RMSE of φ. (c) Overall RMSE of γ. (d) Overall RMSE of η.

From FIGURE 7 and FIGURE 8 we have observed that the proposed CPD-FCM-ALG algorithm yields accurate DOA and polarization estimates in highly and extremely underdetermined cases, if SNR is sufficiently high, while unconstrained CPD does not provide correct results. Note that in the considered cases the unconstrained CPD uniqueness conditions do not hold. We also observe that the optimization based CPD-FCM-QN algorithm provides correct results when it is initialized by the results of CPD-FCM-ALG. The optimization improves the results of CPD-FCM-ALG. However, CPD-FCM-QN dose not yield reasonable estimates

when it is randomly initialized. The above observation has clearly shown the interests in the proposed CPD-FCM-ALG algorithm.

B. RESULTS UNDER PARTIAL CM CONSTRAINT

Here we consider DOA and polarization estimation under partial CM constraint. First, we testify the effectiveness of the proposed CPD-FCM-ALG method against CRB as a benchmark. We fix the number of snapshots to $T = 1000$ and let SNR vary between 0dB and 100dB, the results are given in FIGURE 9.Then, we fix SNR to 20dB and let T vary between 200 and 1000, the results are given in FIGURE 10. We can see that with the increase of SNR or the number of snapshots, the accuracy of CPD-FCM-ALG approaches CRB.

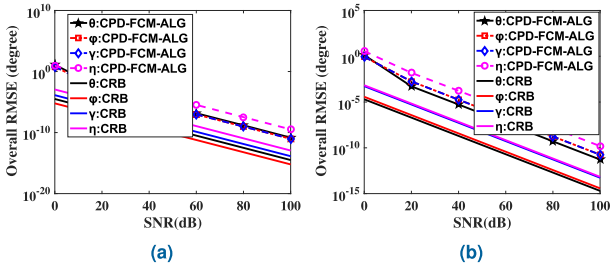

FIGURE 9. Overall RMSE and CRB versus SNR with full CM constraint: $N = K = 3$, $R = 2$, $R_1 == 1$, $T = 1000$. (a) Results with the first source. (b) Results with the second source.

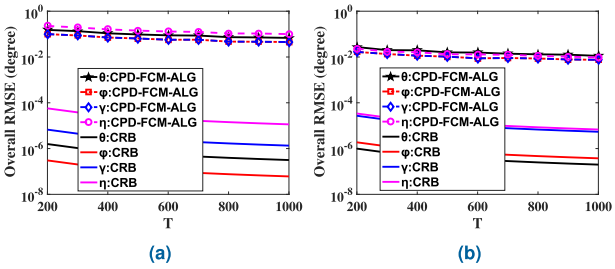

FIGURE 10. Overall RMSE and CRB versus T with full CM constraint: $N = K = 3$, $R = 2$, $R_1 == 1$, $SNR = 20$dB. (a) Results with the first source. (b) Results with the second source.

Now we consider the scenario where only part of the source signals are of CM property. We mainly examine the following two cases: (*i*) a highly underdetermined case $R = 6$, $R_1 = 4$; (*ii*) an extremely underdetermined case $R = 8$, $R_1 = 5$.The corresponding DOA and polarization parameters are set as TABLE 3 and TABLE 4, respectively.

We let SNR vary from 0 dB to 40 dB. The Overall RMSE curves versus SNR for the above two settings are plotted in FIGURE 11 and FIGURE 12, respectively.

From FIGURE 11 and FIGURE 12 we observed that the proposed CPD-PCM-ALG algorithm yields accurate DOA and polarization estimates in highly and extremely underdetermined cases, if SNR is sufficiently high. On the other hand, the unconstrained CPD dose not provide accurate DOA and polarization estimates. First we note that CPD-PCM-QN (RAND) with randomly initialization fails to provide correct

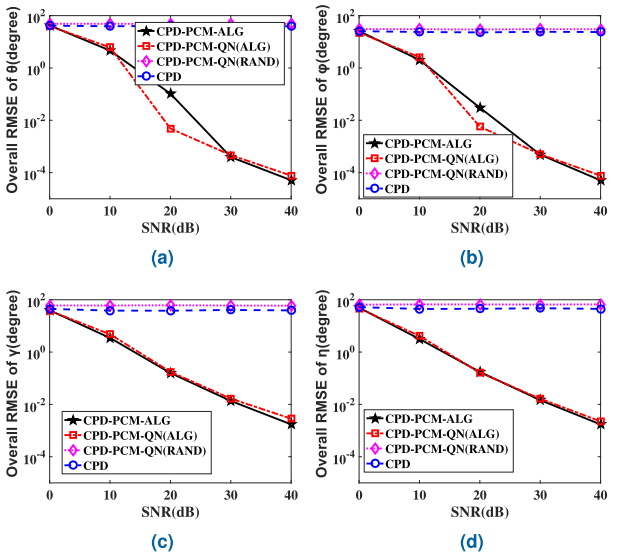

FIGURE 11. Overall RMSE of θ, φ, γ and η versus SNR in the highly underdetermined case with partial CM constraint: $N = K = 3$, $R = 6$, $R_1 = 4$, $T = 1000$. It shows that only CPD-PCM-ALG and CPD-PCM-QN (ALG) yield accurate estimates at medium and high SNR levels. (a) Overall RMSE of θ. (b) Overall RMSE of φ. (c) Overall RMSE of γ. (d) Overall RMSE of η.

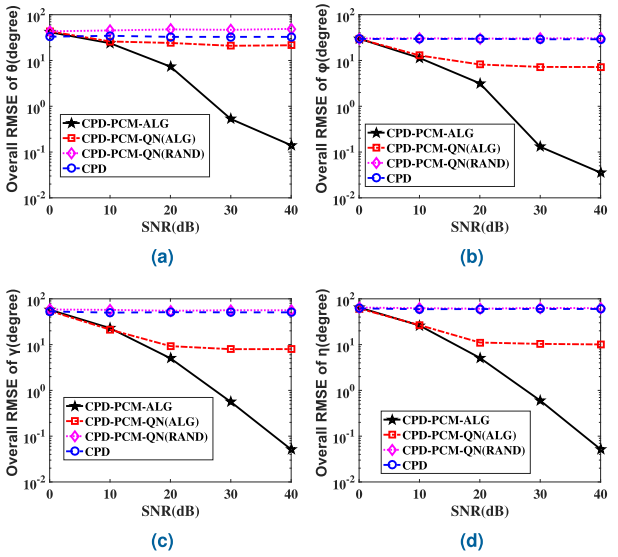

FIGURE 12. Overall RMSE of θ, φ, γ and η versus SNR in the extremely underdetermined case with partial CM constraint: $N = K = 3$, $R = 8$, $R_1 = 5$, $T = 1000$. It shows that only CPD-PCM-ALG yield accurate estimates at high SNR levels. (a) Overall RMSE of θ. (b) Overall RMSE of φ. (c) Overall RMSE of γ. (d) Overall RMSE of η.

results in both case. When it is initialized by the results of CPD-PCN-ALG, we note that CPD-PCM-QN (ALG) yield accurate result in the highly underdetermined case, however, the improvement is not much. We also observed that in the extremely underdetermined case CPD-PCM-QN (ALG) can not generate correct results even it is initialized by the results of CPD-PCM-ALG. This is because in the implementation of CPD-PCM-QN (ALG), we do not incorporate the orthogonality.

In the above simulations, we observe the proposed algorithms are faster than the unconstrained CPD.

V. CONCLUSION

In this study, we have proposed two algebraic algorithms for CPD with two types of CM constraints: CPD-FCM-ALG and CPD-PCM-ALG, which correspond to two scenarios where the sources signals are fully and partially CM, respectively. The proposed algorithms first exploit the analytic CM algorithm to compute the sources matrix, and then use the CPD structure to calculate the rest factor matrices, form which we can obtain the DOA and Polarization parameters. We have shown, through analysis and simulations, that the proposed algorithms have more relaxed uniqueness conditions than unconstrained CPD. In comparison with the optimization based quasi-Newton algorithm, which is shown to be unstable and sensitive to initialization, the proposed algorithms are faster and stable, and can be used to effectively initialize the optimization based algorithms.

REFERENCES

[1] R. Compton, "The tripole antenna: An adaptive array with full polarization flexibility," *IEEE Trans. Antennas Propag.*, vol. AP-29, no. 6, pp. 944–952, Nov. 1981.
[2] A. Nehorai and E. Paldi, "Vector-sensor array processing for electromagnetic source localization," *IEEE Trans. Signal Process.*, vol. 42, no. 2, pp. 376–398, Feb. 1994.
[3] I. Ziskind and M. Wax, "Maximum likelihood localization of diversely polarized sources by simulated annealing," *IEEE Trans. Antennas Propag.*, vol. 38, no. 7, pp. 1111–1114, Jul. 1990.
[4] K. T. Wong and X. Yuan, "'Vector cross-product direction-finding' with an electromagnetic vector-sensor of six orthogonally oriented but spatially noncollocating dipoles/loops," *IEEE Trans. Signal Process.*, vol. 59, no. 1, pp. 160–171, Jan. 2011.
[5] L. L. Monte, B. Elnour, D. Erricolo, and A. Nehorai, "Design and realization of a distributed vector sensor for polarization diversity applications," in *Proc. Int. Waveform Diversity Design Conf.*, Pisa, Italy, Jun. 2007, pp. 358–361.
[6] X.-F. Gong, Z.-W. Liu, and Y.-G. Xu, "Direction finding via biquaternion matrix diagonalization with vector-sensors," *Signal Process.*, vol. 91, no. 4, pp. 821–831, Apr. 2011.
[7] X.-F. Gong, Z.-W. Liu, and Y.-G. Xu, "Coherent source localization: Bicomplex polarimetric smoothing with electromagnetic vector-sensors," *IEEE Trans. Aerosp. Electron. Syst.*, vol. 47, no. 3, pp. 2268–2285, Jul. 2011.
[8] X.-F. Gong, K. Wang, Q.-H. Lin, Z.-W. Liu, and Y.-G. Xu, "Simultaneous source localization and polarization estimation via non-orthogonal joint diagonalization with vector-sensors," *Sensors*, vol. 12, no. 3, pp. 3394–3417, Mar. 2012.
[9] X. Gong, Z. Liu, Y. Xu, and M. I. Ahmad, "Direction-of-arrival estimation via twofold mode-projection," *Signal Process.*, vol. 89, no. 5, pp. 831–842, May 2009.
[10] K. C. Ho, K. C. Tan, and B. Tan, "Efficient method for estimating directions-of-arrival of partially polarized signals with electromagnetic vector sensors," *IEEE Trans. Signal Process.*, vol. 45, no. 10, pp. 2485–2498, Oct. 1997.
[11] Y. Xu, Z. Liu, K. T. Wong, and J. Cao, "Virtual-manifold ambiguity in HOS-based direction-finding with electromagnetic vector-sensors," *IEEE Trans. Aerosp. Electron. Syst.*, vol. 44, no. 4, pp. 1291–1308, Oct. 2008.
[12] E. Ferrara, Jr., and T. Parks, "Direction finding with an array of antennas having diverse polarizations," *IEEE Trans. Antennas Propag.*, vol. 31, no. 2, pp. 231–236, Mar. 1983.
[13] K. T. Wong and M. D. Zoltowski, "Self-initiating MUSIC-based direction finding and polarization estimation in spatio-polarizational beamspace," *IEEE Trans. Antennas Propag.*, vol. 48, no. 8, pp. 1235–1245, Aug. 2000.
[14] K. T. Wong, L. S. Li, and M. D. Zoltowski, "Root-MUSIC-based direction-finding and polarization estimation using diversely polarized possibly collocated antennas," *IEEE Antennas Wireless Propag. Lett.*, vol. 3, pp. 129–132, 2004.
[15] J. Li, "Direction and polarization estimation using arrays with small loops and short dipoles," *IEEE Trans. Antennas Propag.*, vol. 41, no. 3, pp. 379–387, Mar. 1993.
[16] K. T. Wong and M. D. Zoltowski, "Uni-vector-sensor ESPRIT for multisource azimuth, elevation, and polarization estimation," *IEEE Trans. Antennas Propag.*, vol. 45, no. 10, pp. 1467–1474, Oct. 1997.
[17] K. T. Wong and M. D. Zoltowski, "Closed-form direction finding and polarization estimation with arbitrarily spaced electromagnetic vector-sensors at unknown locations," *IEEE Trans. Antennas Propag.*, vol. 48, no. 5, pp. 671–681, May 2000.
[18] M. D. Zoltowski and K. T. Wong, "ESPRIT-based 2-D direction finding with a sparse uniform array of electromagnetic vector sensors," *IEEE Trans. Signal Process.*, vol. 48, no. 8, pp. 2195–2204, Aug. 2000.
[19] M. D. Zoltowski and K. T. Wong, "Closed-form eigenstructure-based direction finding using arbitrary but identical subarrays on a sparse uniform Cartesian array grid," *IEEE Trans. Signal Process.*, vol. 48, no. 8, pp. 2205–2210, Aug. 2000.
[20] K. T. Wong, "Blind beamforming/geolocation for wideband-FFHs with unknown hop-sequences," *IEEE Trans. Aerosp. Electron. Syst.*, vol. 37, no. 1, pp. 65–76, Jan. 2001.
[21] N. D. Sidiropoulos, R. Bro, and G. B. Giannakis, "Parallel factor analysis in sensor array processing," *IEEE Trans. Signal Process.*, vol. 48, no. 8, pp. 2377–2388, Aug. 2000.
[22] X. Guo, S. Miron, and D. Brie, "Identifiability of the parafac model for polarized source mixture on a vector sensor array," in *Proc. IEEE Int. Conf. Acoust., Speech Signal Process.*, Las Vegas, NV, USA, Mar./Apr. 2008, pp. 2401–2404.
[23] X.-F. Gong, Z.-W. Liu, and Y.-G. Xu, "Regularised parallel factor analysis for the estimation of direction-of-arrival and polarisation with a single electromagnetic vector-sensor," *IET Signal Process.*, vol. 5, no. 4, pp. 390–396, Jul. 2011.
[24] M. Sørensen, L. De Lathauwer, P. Comon, S. Icart, and L. Deneire, "Canonical polyadic decomposition with orthogonality constraints," *SIAM J. Matrix Anal. Appl.*, vol. 33, no. 4, pp. 1190–1213, Oct. 2012.
[25] A. Cichocki, R. Zdunek, A. H. Phan, and S. I. Amari, *Nonnegative Matrix and Tensor Factorizations: Applications to Exploratory Multi-Way Data Analysis and Blind Source Separation*. Hoboken, NJ, USA: Wiley, 2009.
[26] M. Sørensen and L. De Lathauwer, "Blind signal separation via tensor decomposition with Vandermonde factor: Canonical polyadic decomposition," *IEEE Trans. Signal Process.*, vol. 61, no. 22, pp. 5507–5519, Aug. 2013.
[27] M. Sørensen and L. D. Lathauwer, "Tensor decompositions with block-Toeplitz structure and applications in signal processing," in *Proc. 45th Asilomar Conf. Signals, Syst. Comput. (ASILOMAR)*, Pacific Grove, CA, USA, Nov. 2011, pp. 454–458.
[28] N. Vervliet, O. Debals, L. Sorber, M. V. Barel, and L. D. Lathauwer. (Mar. 2016). *Tensorlab 3.0*. [Online]. Available: https://www.tensorlab.net/
[29] O. Debals, M. Sohail, and L. De Lathauwer, "Analytical multi-modulus algorithms based on coupled canonical polyadic decompositions," ESAT-STADIUS, KU Leuven, Leuven, Belgium, Tech. Rep. 16-150, 2016.
[30] A.-J. van der Veen and A. Paulraj, "An analytical constant modulus algorithm," *IEEE Trans. Signal Process.*, vol. 44, no. 5, pp. 1136–1155, May 1996.
[31] J.-W. Yang, X.-F. Gong, L.-M. Wang, and Q.-H. Lin, "Canonical polyadic decomposition with constant modulus constraint: Application to polarization sensitive array processing," in *Proc. Int. Symp. Neural Netw. (ISNN)*, Moscow, Russia, Jun. 2019, pp. 575–584.
[32] L. De Lathauwer and J. Castaing, "Tensor-based techniques for the blind separation of DS–CDMA signals," *Signal Process.*, vol. 87, no. 2, pp. 322–336, Feb. 2007.
[33] E. Sanchez, L. S. Ramos, and B. R. Kowalski, "Generalized rank annihilation method: I. Application to liquid chromatography—Diode array ultraviolet detection data," *J. Chromatography A*, vol. 385, pp. 151–164, Jan. 1987.
[34] M. Sorensen and L. De Lathauwer, "New uniqueness conditions for the canonical polyadic decomposition of third-Order tensors," *SIAM J. Matrix Anal. Appl.*, vol. 36, no. 4, pp. 1381–1403, Oct. 2015.

[35] X.-F. Gong, J.-C. Jiang, H. Li, Y.-G. Xu, and Z.-W. Liu, "Spatially spread dipole/loop quint for vector-cross-product-based direction finding and polarisation estimation," *IET Signal Process.*, vol. 12, no. 5, pp. 636–642, Jun. 2018.
[36] L. De Lathauwer, "A link between the canonical decomposition in multilinear algebra and simultaneous matrix diagonalization," *SIAM J. Matrix Anal. Appl.*, vol. 28, no. 3, pp. 642–666, Sep. 2006.
[37] L. Chiantini and G. Ottaviani, "On generic identifiability of 3-tensors of small rank," *SIAM J. Matrix Anal. Appl.*, vol. 33, no. 3, pp. 1018–1037, Sep. 2012.
[38] V. Strassen, "Rank and optimal computation of generic tensors," *Linear Algebra Appl.*, vols. 52–53, no. 1, pp. 645–685, Jul. 1983.
[39] S. Miron, Y. Song, D. Brie, and K. T. Wong, "Multilinear direction finding for sensor-array with multiple scales of invariance," *IEEE Trans. Aerosp. Electron. Syst.*, vol. 51, no. 3, pp. 2057–2070, Jul. 2015.

JIN-WEI YANG received the B.S. degree and the M.S. degree in communication engineering from the Dalian University of Technology, Dalian, China, in 2016 and 2019, respectively.

She is currently with Maoyan Media. Her research interest includes tensor-based array signal processing.

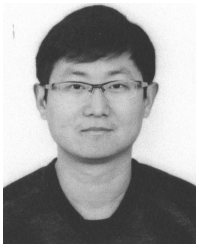

XIAO-FENG GONG (M'10) received the bachelor's degree in information engineering and the joint master's and Ph.D. degree from the Beijing Institute of Technology, China, in 2003 and 2009, respectively, and the Ph.D. degree in communication and information system, in 2009.

From 2014 to 2015, he was a Visiting Research Associate with the KU Leuven Kortrijk Campus, Kortrijk, Belgium. He is currently an Associate Professor with the Dalian University of Technology, Dalian, China. His research interest includes tensor-based signal processing.

CHEN-YU XU received the B.S. degree in communication engineering from Zhengzhou University, Zhengzhou, China, in 2017. She is currently pursuing the M.S. degree with the Dalian University of Technology, Dalian, China.

Her research interest includes tensor-based array signal processing.

QIU-HUA LIN (M'10) received the bachelor's degree in wireless communication, the master's degree in communication and electronic systems, and the Ph.D. degree in signal and information processing from the Dalian University of Technology, Dalian, China, in 1991, 1994, and 2006, respectively.

She was a Teaching Assistant, from 1994 to 1995, a Lecturer, from 1996 to 2001, and an Associate Professor, from 2002 to 2006. She was a Visiting Scholar with the University of New Mexico, Albuquerque, NM, USA, in 2006. She has been with the Dalian University of Technology, since 1994. Since 2007, she has been a Professor with the School of Information and Communication Engineering. Her research interests include array signal processing, biomedical signal processing, image processing, and machine learning.

YOU-GEN XU (M'10) received the M.S. and Ph.D. degrees from the Beijing Institute of Technology, China, in 2001 and 2004, respectively, all in electronic engineering. In September 1998, he joined the Institute of Signal and Image Processing, Beijing Institute of Technology, where he has been involved in projects related to direction finding, digital adaptive robust beamforming, and blind source extraction with advanced vector sensors. Since 2004, he has been with the School of Information and Electronics, Beijing Institute of Technology, where he is currently a Professor. His research interests include array signal processing, wireless sensor networks, regularization methods and applications in sensor array signal processing, biomedical digital signal processing, and space-time adaptive processing. He is a member of the Chinese Institute of Electronics.

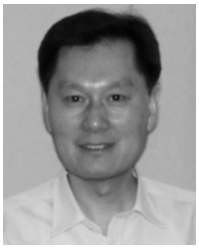

ZHI-WEN LIU (M'10) received the B.S. degree from Xidian University, Xi'an, China in 1983, and the M.S. and Ph.D. degrees from the Beijing Institute of Technology, Beijing, China, in 1986 and 1989, respectively, all in electronic engineering. Since 1989, he has been with the School of Information and Electronics, Beijing Institute of Technology, where he is currently a Professor. His research interests include radar imaging, detection and estimation theory, video image processing, and array signal processing, with applications in communications, radar and life informatics. He is a Senior Member of the Chinese Institute of Electronics. He received the 1995 Distinguished Younger Teacher Award from the Beijing Municipal Government, and the Higher Education Teaching Award from the Beijing Municipal Government, in 2001. He is the Co-Editor of the 1996 CIE International Conference of Radar Proceedings.